Vps34 PI 3-kinase controls thyroid hormone production by regulating thyroglobulin iodination, lysosomal proteolysis and tissue homeostasis

Giuseppina Grieco[1*], Tongsong Wang[1*], Ophélie Delcorte[1*], Catherine Spourquet[1*], Virginie Janssens[1], Aurélie Strickaert[2], Héloïse P. Gaide Chevronnay[1], Xiao-Hui Liao[3], Benoît Bilanges[4], Samuel Refetoff[3], Bart Vanhaesebroeck[4], Carine Maenhaut[2], Pierre J. Courtoy[1*], and Christophe E. Pierreux[1*#]

[1], Cell Biology Unit, de Duve Institute and Université Catholique de Louvain, 1200 Brussels, Belgium;

[2], Institute of Interdisciplinary Research (IRIBHM); Université Libre de Bruxelles, 1070 Brussels, Belgium;

[3], Departments of Medicine (X-H.L., S.R.) and Pediatrics and Genetics (S.R), The University of Chicago, Chicago, Illinois 60637;

[4], UCL Cancer Institute; University College London, 72 Huntley Street, London WC1E 6DD, UK

[#], correspondence to christophe.pierreux@uclouvain.be

*, equal contributions

Running title: Vps34 controls TH synthesis

Key words: Vps34, thyroid, hormone, organification, autophagy

Dr. Giuseppina Grieco, g.pia@hotmail.it

Dr. Tongsong Wang, tswang0802@hotmail.com

Ms. Ophélie Delcorte, ophelie.delcorte@uclouvain.be

Ms. Catherine Spourquet, catherine.spourquet@uclouvain.be

Ms. Virginie Janssens, virginie.janssens@uclouvain.be

Dr. Aurélie Strickaert, aurelie.strickaert@ulb.ac.be

Dr. Héloïse Gaide-Chevronnay, heloisegaide@hotmail.com

Dr. Xia Hui Liao, xliao1@uchicago.edu

Dr. Benoit Bilanges, b.bilanges@ucl.ac.uk

Prof. Samuel Refetoff, srefetof@uchicago.edu

Prof. Bart Vanhaesebroeck, bart.vanh@ucl.ac.uk

Prof. Carine Maenhaut, cmaenhau@ulb.ac.be

Prof. Pierre J. Courtoy, pierre.courtoy@uclouvain.be

Prof. Christophe E. Pierreux, christophe.pierreux@uclouvain.be

Abstract (327 words, 350 allowed)

BACKGROUND: The production of thyroid hormones (T_3, T_4) depends on the organization of the thyroid in follicles, which are lined by a monolayer of thyrocytes with strict apico-basal polarity. This polarization supports vectorial transport of thyroglobulin for storage into, and recapture from, the colloid. It also allows selective addressing of channels, transporters, ion pumps and enzymes to their appropriate basolateral (NIS, SLC26A7 and Na^+/K^+-ATPase) or apical membrane domain (Anoctamin, SLC26A4, DUOX2, DUOXA2 and TPO). How these actors of T_3/T_4 synthesis reach their final destination remains poorly understood. The PI 3-kinase (PI3K) isoform Vps34/PIK3C3 is now recognized as a main component in the general control of vesicular trafficking and of cell homeostasis via the regulation of endosomal trafficking and autophagy. We recently reported that conditional Vps34 inactivation in proximal tubular cells in the kidney prevents normal addressing of apical membrane proteins and causes abortive macroautophagy.

METHODS: Vps34 was inactivated using a Pax8-driven Cre recombinase system. The impact of Vps34 inactivation in thyrocytes was analyzed by histological, immunolocalization and mRNA expression profiling. Thyroid hormone synthesis was assayed by ^{125}I injection and serum plasma analysis.

RESULTS: $Vps34^{cKO}$ mice were born at the expected Mendelian ratio and showed normal growth until postnatal day 14, then stopped growing and died at around 1 month of age. We therefore analyzed thyroid $Vps34^{cKO}$ at postnatal day 14. We found that loss of Vps34 in thyrocytes causes: (i) disorganization of thyroid parenchyma, with abnormal thyrocyte and follicular shape and reduced PAS^+ colloidal spaces; (ii) severe non-compensated hypothyroidism with extremely low T_4 levels (0.75 ± 0.62 μg/dL) and huge TSH plasma levels

(19,300 ± 10,500 mU/L); (iii) impaired ^{125}I organification at comparable uptake and frequent occurrence of follicles with luminal thyroglobulin but non-detectable T4-bearing thyroglobulin; (iv) intense signal in thyrocytes for the lysosomal membrane marker, LAMP-1, as well as thyroglobulin and the autophagy marker, p62, indicating defective lysosomal proteolysis, and (v) presence of macrophages in the colloidal space.

CONCLUSIONS: We conclude that Vps34 is crucial for thyroid hormonogenesis, at least by controlling epithelial organization, Tg iodination as well as proteolytic T_3/T_4 excision in lysosomes.

72 ***Introduction***

73 The main function of the thyroid gland is to produce the hormones, T_3/T_4 and
74 calcitonin, which are essential for the regulation of metabolic processes (1,2). The production
75 of T_3 and T_4 depends on the correct tissue organization of thyroid epithelial cells, the
76 thyrocytes, into functional and independent units, the follicles. These are composed of a single
77 layer of polarized thyrocytes that form a spherical structure delineating an internal space or
78 lumen where the thyrocyte secretory product, thyroglobulin, is stored in a colloidal form, thus
79 called the colloid lumen. As thyrocytes communicate via gap junctions, each follicle functions
80 as an integrated unit. Thyroid hormone synthesis depends on apico-basal cell polarity that
81 allows the specific localization of channels, transporters, pumps and enzymes at the
82 appropriate membrane domains. Iodide from the bloodstream freely traverses the
83 fenestrated endothelium of the thyroid capillaries and is taken up into thyrocytes via the
84 basolaterally-localized Na^+/I^- symporter (NIS), thanks to a Na^+ gradient generated by the
85 Na^+/K^+-ATPase. An alternative basolateral transporter, SLC26A7, has been recently reported
86 to also control iodide uptake, although its role might be indirect (3). Iodide diffuses freely
87 within thyrocytes and is next transported across the apical membrane into the colloid space
88 via apically-localized transporters such as anoctamin or pendrin (SLC26A4). Iodide is then
89 rapidly oxidized into iodine by thyroperoxidase (TPO) located at the apical membrane, in the
90 presence of H_2O_2, generated by the DUOX2/DUOXA2 apical membrane complex. Iodine is
91 incorporated into accessible tyrosine residues close to the N- and C-termini of thyroglobulin
92 (Tg), a large protein secreted by thyrocytes into the colloid space. Iodotyrosine rearranges into
93 hormonogenic peptides, which are the direct T_3 and T_4 precursors. Thyroid hormone synthesis
94 thus requires basal localization of NIS, SLC26A7 and Na^+/K^+-ATPase, apical localization of
95 anoctamin, pendrin, TPO, DUOX2 and DUOXA2, as well as apical delivery of Tg into the colloid

96 lumen and endocytic uptake of iodoTg into thyrocyte lysosomes (1,2). Specific regulators of
97 thyroid follicular organization have recently been identified (4). Transcriptomic comparison of
98 thyroid FRT cells cultured in 2D monolayers and in 3D spherical follicles indeed revealed
99 involvement of structural and functional cell elements such as adherens and tight junctions
100 (cadherin-16), cytoskeleton proteins, ions channels, proteins involved in differentiation, and
101 components of the trafficking machinery (e.g. myosin-Vb, Rab17) (4).

102 There is strong evidence that vesicular trafficking is critical for apico-basal polarization
103 and epithelial function (5-7), but the role of vesicular trafficking in thyroid function is
104 incompletely understood. Vps34/*PIK3C3* (also referred to as type III PI3K) has long been
105 recognized as a main actor involved in the general control of endocytic vesicular trafficking (8-
106 13). Vps34/PIK3C3 also plays an important role in epithelial organization in *Drosophila* (14)
107 and in autophagy (12,15), both in the initiation of autophagosome formation and the
108 progression towards autophagosome-lysosome fusion (16,17).

109 We recently inactivated Vps34 in kidney proximal tubular cells (PTC) using Wnt4-Cre
110 and Pax8-Cre (18,19). Wnt4-Cre driven Vps34 excision caused major perinatal lethality, with
111 abnormalities in kidney cortex development and PTC apical differentiation in the surviving
112 mice. With the Pax8-Cre, which triggers recombination in nephrogenic tubules and in
113 nonvascular components of glomeruli two days later than Wnt4-Cre (20,21), we observed
114 normal mouse growth until postnatal (P) day 14 (19). Then, body weight levelled off and all
115 pups died at ~3-5 weeks of age, probably due to kidney failure. Structural and functional
116 studies of Vps34^{cKO} kidneys revealed preserved PTC membrane polarity, but impaired apical
117 membrane protein trafficking, thus causing a general PTC dysfunction known as renal Fanconi-
118 like syndrome, manifested by polyuria and low-molecular weight proteinuria. Vps34^{cKO} also
119 displayed impaired lysosome size/positioning and blocked autophagy, thereby causing cell

120 vacuolization. We concluded that Vps34 is a crucial component of the trafficking machinery
121 necessary for differentiated PTC function and is essential for overall PTC homeostasis (19).
122 Given that Pax8-Cre also triggers recombination in thyrocytes (21), we here investigated the
123 role of Vps34/PIK3C3 in thyroid function and homeostasis.

124 ***Materials and methods***

125 *Mice*

126 Vps34$^{fl/fl}$ mice have been described (22). Pax8-Cre mice were obtained from Dr. M.
127 Busslinger (21). Vps34$^{fl/fl}$ mice were crossed with Pax8-Cre;Vps34$^{fl/+}$ mice to generate
128 conditional targeted excision of Vps34 exon 21 in the thyroid of 25% of offspring (Vps34^{cKO}).
129 Non-recombined Vps34$^{fl/fl}$ mice were used as control. Mice were treated according to the NIH
130 Guide for Care and Use of Laboratory Animals, and experiments were approved by the
131 University Animal Welfare Committee, Université Catholique de Louvain (2016/UCL/MD/006
132 and 2018/UCL/MD/026).

133 *Plasma, tissue collection and histology*

134 Blood was collected by eye sinus puncture at sacrifice (P14) under irreversible
135 anesthesia by xylazine 2% and ketamine 50 mg/ml (200 l/mice i.p.). Thyroid lobes were
136 excised, fixed by immersion in neutral-buffered formaldehyde (4% F) at 4°C under stirring
137 overnight. Samples were paraffin-embedded or equilibrated overnight in 20% sucrose and
138 embedded in Tissue-Tek Optimal Cutting Medium (Sakura Finetek) for cryostat sections.

139 *TSH and T4 plasma concentrations*

140 Plasma TSH concentrations were measured by a sensitive, heterologous,
141 disequilibrium double-antibody precipitation RIA as described (23). T4 concentration was
142 measured by coated-tube RIA (Siemens Medical Solution Diagnostics, Los Angeles, CA).

143 *Immunofluorescence*

144 Immunofluorescence was performed on 5 µm-thick frozen sections or on 6 µm-thick
145 paraffin sections (19). Antigen retrieval was promoted in citrate buffer, pH 6.0, at 98°C for 20
146 min using a Lab Vision Pretreatment Module™ (Thermo Scientific). After permeabilization with
147 PBS/0.3% Triton-X100 for 5 min, non-specific sites were blocked by 1-h incubation in PBS/0.3%
148 Triton-X100 with 10% bovine serum albumin (BSA) and 3% milk, followed by primary
149 antibodies (described in Supplementary Table I) in blocking buffer at 4°C overnight. After
150 extensive washing, sections were incubated with the appropriate AlexaFluor-secondary
151 antibodies in 10% BSA/0.3% Triton-X100 at room temperature for 1 h, extensively washed,
152 mounted with Faramount Aqueous Mounting Medium (Dako) and imaged on a spinning disk
153 confocal microscope using a Plan Apochromat 100x/1.4 Oil DIC objective (Cell Observer
154 Spinning Disk; Zeiss). For whole thyroid section recording, images were acquired using Zeiss
155 Pannoramic P250 slide scanner, stitched and analyzed using Case Viewer software.

156 *RT-qPCR*

157 Total RNA was extracted from thyroid lobes using TRIzol Reagent (Thermo Scientific),
158 as described (24). Aliquots of 500 ng RNA were reverse-transcribed by M-MLV reverse
159 transcriptase (Invitrogen) with random hexamers, as described (25). Primer sequences used
160 are described in Supplementary Table II. Real-time qPCR was performed as described (25), in
161 presence of 250 nM of specific primers with Kappa SYBR Fast qPCR Master Mix (Kapa
162 Biosystems) on a CFX96 touch real-time PCR Detection System (Bio-Rad). Data were analyzed

163 using the ΔΔCT method, using the geometric mean of β-*Actin* and *Rpl27* as reference genes
164 (26).

165 *^{125}I uptake and organification*

166 At postnatal day 8 (P8), mothers and litters were fed with an iodine-free diet for 24 h.
167 At P9, pups were injected intraperitoneally with 1 µCi ^{125}I (Perkin Elmer) and left for another
168 24 h before sacrifice and thyroid dissection. Both lobes were collected in 2 mM methimazole
169 (Sigma) and homogenized with a glass Potter. Total thyroid ^{125}I was measured with an
170 automatic gamma counter "Wizard^{2}" (Perkin Elmer) before protein precipitation using 10%
171 trichloroacetic acid (TCA; Merck). After a single wash in TCA, radioactivity was measured in
172 the protein pellet. Percentage of protein-bound iodide was calculated using the ratio of
173 precipitated cpm/total thyroid cpm (27).

174 *H_2O_2 level measurements*

175 The hydrogen peroxide Assay kit from Abcam (ab102500) was used. At P14, thyroid
176 lobes were collected in ice-cold PBS and homogenized with a glass Potter. Proteins were
177 precipitated with perchloric acid 4 M, and supernatant was neutralized with KCl 3 M and KCl
178 1 M until pH was comprised between 6.5 and 8. Fifty µl, corresponding to a ninth of a thyroid,
179 was incubated with OxiRed probe and horseradish peroxidase (HRP), according to the
180 instructions form the manufacturer. Fluorescence was measured with a GloMax fluorimeter
181 (Promega, Ex/Em = 535/587 nm).

182 *Statistical analysis*

183 All statistical analyses were determined by Prism software (GraphPad Software, La
184 Jolla, California, USA). RT-qPCR values were obtained by the ΔΔCT method and are expressed

185 as boxplots with median, 25th and 75th percentiles, and min-max whiskers. Each graph
186 represents the results form a minimum of 8 independent thyroid lobes from at least 3
187 different litters. Nonparametric statistical tests were used: Mann-Whitney for single
188 comparisons. Differences were considered statistically significant when $p<0.05$ (*); ** stands
189 for $p<0.01$; *** for $p<0.001$.

190 ***Results***

191 *Genetic construction and assessment of Vps34 inactivation*

192 Ubiquitous Vps34 inactivation is embryonically lethal, with embryos dying around
193 embryonic day E8.5 (28). To study tissue-specific roles of Vps34 *in vivo,* we used a mouse line
194 which carries a floxed *Vps34* allele (Vps34^{fl}) that allows to conditionally delete the loxP-flanked
195 exon 21 of the *Vps34* gene, which encodes a critical sequence of the lipid kinase domain of
196 Vps34 (22). This approach was designed to allow for the expression of a minimally-truncated,
197 catalytically-inactive Vps34 protein. However, upon conditional expression in
198 megakaryocytes, the level of this truncated Vps34 and its obligatory partner, Vps15, were
199 found to be decreased by 80-90% in the megakaryocyte lineage (thrombocytes), indicating
200 instability of truncated Vps34 protein (22). We will thus hereafter refer to the result of this
201 Vps34 truncation as Vps34 conditional knock-out (Vps34^{cKO}).

202 We crossed homozygous Vps34$^{fl/fl}$ mice with Pax8-Cre;Vps34$^{fl/+}$ mice, which is expected
203 to lead to a tissue-specific (thyroid and kidney) conditional excision of exon 21 from both
204 Vps34 alleles in 25% of the pups, which are further referred to as Vps34^{cKO} mice. Vps34^{cKO}
205 mice were born at the expected Mendelian ratio and showed normal development until
206 postnatal day 14 (P14), then stopped growing and died at around 1 month of age (19). We

207 therefore analyzed the thyroid of Vps34^{cKO} mice at P14. Of note, eye opening, a marker of
208 cerebral maturation was usually delayed till P10.

209 We first assessed the extent of Vps34 genetic excision in the thyroid by quantification
210 of *Vps34* mRNA using primer that are specific for the total *Vps34* or are exon 21-specific.
211 Compared to control littermate pups, we found a ~70 % reduction of exon 21-containing
212 *Vps34* mRNA in cKO thyroid extracts. In comparison, we found no significant difference in the
213 abundance of *Vps34* mRNA containing exon 22-24 (Fig. 1A). Assuming that *Vps34* is equally
214 expressed in all thyroid cell types (expressing and non-expressing the Cre recombinase), this
215 ~70 % decrease suggests that most thyrocytes in Vps34^{cKO} mice had undergone Cre-mediated
216 recombination.

217 *Vps34^{cKO} thyroids show signs of hyperstimulation by thyroid stimulating hormone (TSH)*

218 At P14, thyroid glands from Vps34^{cKO} were almost twice heavier as compared to
219 control glands (Fig. 1B). Histological staining using Periodic-Acid-Schiff (PAS, which in the
220 thyroid reflects production of the thyroglobulin glycoprotein) readily revealed striking
221 differences between thyroid glands of control and Vps34^{cKO} mice (Fig. 1C). Thyroid glands of
222 control mice appeared as assemblies of round follicular sections of variable diameter, filled
223 with colloid intensely and homogenously stained by PAS. Although histology of Vps34^{cKO} was
224 more variable, the three representative individual thyroids shown in Fig. 1C revealed irregular
225 follicle shape, especially at the periphery of the gland, and weaker or absent PAS staining (Fig.
226 1C and Suppl. Fig. 1). In addition, the PAS-negative follicular space were often filled with nuclei
227 (see Vps34^{cKO} #3). Quantification revealed that 90% of control follicles had a regular shape
228 and intense (+++) PAS staining (Suppl. Fig. 1). On the contrary, only 50% of Vps34^{cKO} follicles
229 displayed a regular shape and most of the follicles were weakly positive for PAS (++ or +)

230 (Suppl. Fig. 1). In addition, 10 to 50% of the Vps34^{cKO} follicles showed no PAS staining (-) and
231 luminal cells were found in 40-70% of the follicles (Suppl. Fig. 1). Confocal
232 immunofluorescence microscopy for the epithelial marker E-cadherin confirmed
233 heterogeneity of Vps34^{cKO} follicles, but also of thyrocytes. Hoechst labelling revealed the
234 presence of several nuclei in a significant fraction of lumina (Fig. 1D). These histological
235 features of follicle remodelling and colloid consumption up to exhaustion, suggested
236 perturbed thyroid function.

237 *Vps34^{cKO} causes severe non-compensated hypothyroidism*

238 To directly test the hypothesis that Vps34^{cKO} could impair thyroid hormone production,
239 plasma was collected at P14 and analyzed for the levels of T_4 and TSH. In P14 control pups,
240 values were 6.4 ± 1.5 μg/dL for T_4, and 75 ± 110 mU/L for TSH (Fig. 2). In Vps34^{cKO} mice, we
241 found extremely low T_4 values (0.75 ± 0.62 μg/dL) and very high plasma levels of TSH (19,311
242 ± 10,482 mU/L) (Fig. 2). These data indicate severe, non-compensated hypothyroidism. This
243 observation, compatible with the growth retardation observed after P15 (19), could be
244 explained by mislocalization of one or several basolateral and/or apical actors involved in
245 thyroid hormone synthesis, as we reported in Vps34^{cKO} kidney proximal tubular cells (19).

246 *Vps34 cKO display reduced iodine organification*

247 The reduced or absent PAS staining (Fig. 1C) and the low T_4 plasma levels in Vps34^{cKO}
248 mice (Fig. 2) might be caused by defective basolateral iodine uptake, apical transport and/or
249 apical organification on thyroglobulin. Due to lack or very poor specificity of antibodies
250 directed against murine proteins involved in these processes, we first measured their mRNA
251 expression levels in total thyroids at P14 (Fig. 3). We observed no change in mRNA expression
252 of *Nis*, *Ano1*, *Tg*, *Tpo* and *Duox2,* a significant increase in *Tshr* and *Slc26a4* expression, and a

253 significant decrease of *Slc26a7* and *Duoxa2* mRNA levels. At this stage, we cannot conclude if
254 these changes contribute to the observed hypothyroidism of Vps34^{cKO}.

255 To further test whether basolateral NIS and SLC26A7 and apical ANO1, SLC26A4, TPO,
256 DUOX and DUOXA were all correctly localized, we functionally assayed their combined activity
257 by injecting iodine-deprived pups at P9 with ^{125}I. At P10, 24-h post-injection, thyroid lobes
258 were collected and radioactivity measured before and after protein precipitation by TCA (Fig.
259 4A). ^{125}I uptake was not statistically-different in Vps34^{cKO} and the three control genotypes (Fig.
260 4A), suggesting normal NIS and SLC26A7 function and thus basolateral localization. In marked
261 contrast, only 10% of thyroid ^{125}I was bound to proteins in Vps34^{cKO} compared to
262 approximately 55% in control genotypes at this stage (Fig. 4A). This indicates a major effect of
263 Vps34 on one or several apical proteins involved in iodine organification.

264 Normal *Ano1* and increased *Slc26a4/Pendrin* mRNA levels suggested correct, or even
265 improved, transfer of iodine in the follicular lumen. On the other hand, decreased *Duoxa2*
266 might impact on H_2O_2 production. We thus measured the production of H_2O_2 in control and
267 Vps34^{cKO} thyroid lobes. Surprisingly, the median level of H_2O_2 production in Vps34^{cKO} was
268 higher, even if we observed variability (Fig. 4B), indicating that the DUOX/DUOXA pair is
269 functional in Vps34^{cKO} thyroid. Altogether, these results suggest defective localization of one
270 or several apical actors involved in iodine organification.

271 *Apical polarity is impaired in Vps34^{cKO}*

272 Apico-basal polarity is essential for thyrocyte function and defects in polarity might
273 impact on the delivery, and thus localization, of actors involved in thyroid hormone synthesis.
274 As general markers to assess polarity, we used the basement membrane protein laminin, the
275 basolateral Na^+/K^+-ATPase, E-cadherin and β-catenin, the apically-localized ERM family

276 member ezrin and the tight junction-associated protein ZO-1. Control thyrocytes displayed a
277 well-defined apico-basal polarity with laminin assembled on the basal side, with Na^+/K^+-
278 ATPase, E-cadherin and β-catenin restricted to the basolateral membrane and separated from
279 apical ezrin by the tight junction, visualized by ZO-1 (Fig. 5A and 5B). In $Vps34^{cKO}$ thyrocytes,
280 basal laminin was correctly assembled and Na^+/K^+-ATPase, E-cadherin and β-catenin were
281 restricted to the basolateral membrane, indicating the presence of functional tight junctions.
282 However, on the apical side of $Vps34^{cKO}$ thyrocytes, the ezrin signal was weaker or absent from
283 the lumen-facing pole of some thyrocytes (Fig. 5A), and most cells also lacked ZO-1 protein
284 labelling (Fig. 5B). These data suggest impaired apical polarity in $Vps34^{cKO}$, which might
285 contribute to defective localization of apical actors involved in iodine organification.

286 *$Vps34^{cKO}$ mice display defective thyroglobulin iodination*

287 To further analyse the significance of the lack of PAS staining in a fraction of $Vps34^{cKO}$
288 follicles (Fig. 1C) and the defect in iodine organification (Fig. 4), we assessed thyroglobulin
289 protein expression and its associated T_4 hormonogenic peptide (I-Tg) by immunofluorescence.
290 Low magnification of control sections showed an identical distribution pattern of
291 thyroglobulin and I-Tg, homogeneously filling all round colloidal spaces (Fig. 6A). In $Vps34^{cKO}$,
292 the thyroglobulin labelling was more heterogeneous, mainly due to the presence of cells in
293 the colloid. Remarkably, antibodies recognizing the T_4 hormonogenic peptide often failed to
294 label colloidal spaces even when containing Tg in the adjacent section (Fig. 6A), thereby
295 confirming the organification defect (Fig. 4A). Quantification revealed that only a quarter (25.2
296 ± 11.9 %) of the follicles were labeled for T_4 hormonogenic peptide. Of specific interest,
297 whereas the Tg signal was restricted to the follicle lumen in control thyroid, high magnification
298 revealed that the Tg signal was frequently seen within $Vps34^{cKO}$ thyrocytes (Fig. 6B,

299 arrowheads). These observations indicated that Vps34 deletion caused defective
300 thyroglobulin iodination, as well as reduced Tg exocytosis and/or excessive Tg endocytosis.

301 *Impaired lysosomal function and I-Tg proteolysis in Vps34^{cKO} thyroid*

302 Vps34 is involved in endocytic trafficking and cKO of Vps34 in postnatal kidney
303 glomeruli podocytes causes a strong increase of the overall immunofluorescence signal for
304 the lysosomal membrane marker LAMP-1, indicating enhanced lysosome biogenesis (29,30).
305 We further reported that absence of Vps34 in kidney PTCs causes an increase in the actual
306 size of lysosomes, that were sometimes enlarged, and mislocalized toward the basal pole of
307 the cell (19). Given that lysosomal proteases in thyrocytes are important to excise
308 hormonogenic peptides to release free T_3 and T_4, we investigated LAMP-1-labeled structures
309 in Vps34^{cKO} thyrocytes as a proxy for lysosomal function, and its co-localization with Tg and I-
310 Tg to demonstrate endocytosis. In our conditions, immunofluorescence on control thyroid
311 sections only produced a weak LAMP-1 signal in the E-cadherin-positive epithelial thyrocytes
312 (Fig. 7A and 7B). On the contrary, a strong and widespread LAMP-1 signal was observed in all
313 Vps34^{cKO} thyrocytes. As shown in the enlarged boxes of Fig. 7A and 7B (separate emission
314 channels in white), LAMP-1-positive late endosomes/lysosomes were more abundant, and
315 sometimes enlarged in Vps34^{cKO} thyrocytes as compared to control. In addition, the
316 intracellular Tg protein, found in most Vps34^{cKO} thyrocytes (Fig. 7A, arrowheads), most often
317 colocalized with LAMP-1-positive structures. This indicates that colloidal Tg was endocytosed
318 by thyrocytes, but that trafficking to or Tg proteolysis within the lysosomes was slower or
319 impaired, as compared to controls. Of note, luminal cells also contained LAMP-1 structures
320 positive for Tg (Fig. 7A, right).

321 Additional supporting evidence for impaired lysosomal proteolysis came from the
322 analysis of I-Tg (Fig. 7B). Indeed, Vps34^{cKO} thyrocytes often contained intracellular signal for I-
323 Tg, colocalizing within LAMP-1 structures (Fig. 7B, enlarged boxes,). Thus, in addition to
324 reduced iodine organification, defective lysosomal proteolysis of T_3/T_4, if/when hormonogenic
325 peptides were still formed on Tg, was also accounting for the low T_3/T_4 plasma levels observed
326 in Vps34^{cKO} (Fig. 2).

327 *Evaluation of autophagy in Vps34^{cKO} thyroid*

328 The deletion of Vps34 in the kidney also causes a block of autophagy (19). We therefore
329 assessed the expression of p62 (also called sequestosome-1, or SQSTM1), a polyubiquitin-
330 binding protein that interacts with LC3b (microtubule associated protein 1 light chain) on the
331 autophagosome membrane and is normally continuously degraded by the autophagy process
332 (31). Since p62 accumulates when completion of autophagy is inhibited, p62 can be used as a
333 marker to study autophagic flux (32). Although we found a weak punctiform LC3 signal in
334 control thyrocytes, we observed no p62 signal, indicating normal autophagic flux in control
335 thyroid. As reported, few LAMP-1-labelled structures were found in control thyroid. In
336 contrast, much larger structures, mostly double-labeled for p62 and LC3, were easily detected
337 in the cytoplasm of Vps34^{cKO} thyrocytes. As the LAMP-1 signal was increased in Vps34^{cKO}, these
338 p62/LC3-positive punctae sometimes co-localized with LAMP-1. We concluded that LC3 could
339 be recruited on p62 aggregates but that progression to autophagosome maturation and fusion
340 with, and degradation by, lysosomes was arrested. This suggested that deletion of Vps34 in
341 thyrocytes abrogated the autophagic flux.

342 Recent evidences have demonstrated that p62 is also an activator of the antioxidant
343 KEAP1/NRF2 pathway, which impacts on thyrocyte physiology and Tg biology (33). We thus

344 examined the possibility that stabilized p62 would compete with NRF2 for KEAP1 binding in
345 Vps34^{cKO}, thus allowing NRF2 to reach the nucleus and activate gene expression. We
346 quantified the mRNA levels of *Nrf2* and its target genes *Nqo1*, *Gpx2* and *Txnrd1*. Although we
347 measured a slight decrease of *Nrf2* mRNA in Vps34^{cKO}, two of its target genes, namely the
348 quinone reductase, *Nqo1*, and the thioredoxin reductase 1, *Txnrd1*, were upregulated 1.9- and
349 3.5-fold, respectively (Fig. 8B). This observation supports the hypothesis that KEAP1
350 interaction with p62 is favored in Vps34^{cKO} and that NRF2 is thus displaced and able to migrate
351 to the nucleus to regulate gene expression.

352 We also evaluated macroautophagy/mitophagy by immunolocalizing TOM20 and
353 LAMP-1. In Vps34^{cKO} thyrocytes, TOM20-labeled structures did not colocalize with the more
354 abundant, enlarged LAMP-1+ structures (Suppl. Fig. 2A), as we also reported in Vps34^{cKO}
355 kidney proximal tubular cells (19). This suggested that sequestration of mitochondria into
356 autophagosomes is either not triggered, which is unlikely for altered cells, or abortive at P14
357 in Vps34^{cKO} thyrocytes, and/or that fusion of autophagosomes with lysosomes is prevented.
358 We then evaluated the chaperone-mediated autophagy by immunolocalizing LAMP-2A. As
359 compared to control thyroid, LAMP-2A-labeled structures were more abundant in Vps34^{cKO}
360 thyrocytes (Suppl. Fig. 2B), as we also reported in Vps34^{cKO} kidney proximal tubular cells (19).

361 *Luminal cells present in Vps34^{cKO} follicles are macrophages*

362 Finally, we investigated the origin of the cells present in the colloidal space. As
363 observed in Figure 7A, cells trapped in the follicular lumen showed a strong LAMP-1 signal
364 (Fig. 7A). However, they were negative for E-cadherin (Figs. 1D and 5A). In addition, we found
365 that luminal cells were also negative for the permanently-expressed thyrocyte-specific
366 transcription factor, TTF-1 (Fig. 9A), indicating that these cells were not derived from the

367 thyrocyte lineage. Lineage-tracing experiments on Pax8-Cre; Vps34$^{fl/fl}$;ROSA-STOP-YFP pups at
368 P14 further revealed YFP-positive signal only in follicle-delineating thyrocytes and not in the
369 luminal cells (Fig. 9B). Thus, luminal cells had never expressed Pax8 and were thus not derived
370 from thyrocyte progenitors. Although infiltration by C-cells was a possibilty, we failed to label
371 luminal cells for the Prox1 transcription factor. As luminal cells displayed LAMP-1 signal and
372 were also positive for Tg (Fig. 7A), we tested the possibility that luminal cells were infiltrating
373 macrophages. This was the case: luminal cells were labeled by the macrophage marker F4/80
374 (Fig. 10A), but not by E-cadherin. To confirm that colloid was consumed by infiltrated
375 macrophages, we performed a triple immunolabelling for F4/80, LAMP-1 and I-Tg. Luminal
376 F4/80-positive cells displayed huge LAMP-1-positive lysosomes filled with I-Tg (Fig. 10B). Thus,
377 colloid consumption (Tg in Fig. 7A and I-Tg in Fig. 9D) by infiltrated macrophages provides a
378 third explanation for the low T_4 plasma level observed in Vps34^{cKO}.

379 ***Discussion***

380 In this study, we report that deleting Vps34 in thyrocytes by Pax8-Cre-driven
381 recombination causes several defects in the thyroid: (i) doubling of thyroid weight and
382 perturbed thyroid parenchyma organization, with reduced PAS^{+} colloidal spaces; (ii) severe
383 hypothyroidism with collapsed plasma T_4 levels and very high TSH; (iii) strong decrease of ^{125}I
384 organification, at comparable ^{125}I uptake, and of T_4 formation on thyroglobulin (detected by
385 immunofluorescence as early as P3); (iv) defective apical polarization; (v) impaired lysosomal
386 proteolysis; (vi) infiltration of macrophages in the colloid. Some of these features, combined
387 with delayed "eye opening" and impaired postnatal growth after two weeks (18), phenocopy
388 the impact of *Duoxa2* KO in the thyroid (34).

389 DUOXA2 is a chaperone protein required for the correct localization of DUOX2 at the
390 apical pole of thyrocyte, where the complex (DUOX2/DUOXA2) produces H_2O_2. In the absence
391 of DUOXA2, H_2O_2 is not produced and subsequent thyroperoxidase-mediated oxidation of
392 iodide into reactive compounds and thyroglobulin iodination are abolished (34). The similarity
393 of the severity of hypothyroidism in Vps34^{cKO} and *Duoxa2* KO mice prompted us pay a closer
394 look at DUOXA2 in Vps34^{cKO}. We found that the expression of *Duoxa2* started decreasing after
395 P3, reaching two-fold lower values at P14. It is interesting to note that expression of *Duox2*
396 and *Duoxa2* mRNAs was quantitatively different, despite of the fact that they share the same
397 promoter (35). Whether decreased *Duoxa2* mRNA expression is reflected by equivalent two-
398 fold decrease of DUOX2/DUOXA2 complex at the apical pole is unknown. However, it is very
399 unlikely that a two-fold decrease would by itself so severely impact on thyroglobulin
400 iodination, since heterozygous mice for *Duoxa2* deletion have virtually no phenotype. In
401 addition, our measurements of H_2O_2 levels in total Vps34^{cKO} thyroid extracts also support
402 normal, or increased, function of the DUOX2/DUOXA2 complex. Instead, based on the known
403 functions of Vps34 in kidney PTCs, where its inactivation causes lack of apical localization of
404 endocytic receptors (megalin, cubilin) and solute transporters (NaPi-IIa, SGLT-2) (19), it would
405 be extremely interesting to localize actors of thyroid hormonogenesis on thyroid sections, and
406 assess their basolateral or apical addressing in Vps34^{cKO} thyrocytes. Unfortunately, reliable
407 antibodies to detect most of these proteins are not yet available for mice. Nevertheless, ^{125}I
408 uptake and processing experiments suggests normal localization and function of the sodium-
409 iodine symporter, NIS, and/or the alternative transporter SLC26A7 (3), and rather support the
410 hypothesis of defective apical localization of one or several actors involved in thyroid
411 hormonogenesis (Ano1, pendrin, TPO, DUOX, DUOXA).

412 Characteristic histopathological alterations combined with the very high plasma TSH
413 levels and two-fold increased *Tshr* expression in Vps34^{cKO} thyroid suggest that thyrocytes are
414 in a hyperstimulated state. For example, DuoxA2 KO, which display very high TSH levels,
415 present a 20- and 5-fold higher expression level of *Nis* and *Tpo*, as compared to controls (34).
416 However, the expression of these two sensitive target genes of the TSH signaling pathway, *Nis*
417 and *Tpo*, was surprisingly unchanged in Vps34^{cKO}, arguing against thyrocyte hyperstimulation.
418 We favor the hypothesis of TSHR mistrafficking into intracellular vesicles. Recent work in
419 *Drosophila* revealed that Vps34 inactivation or pharmacological inhibition using the small
420 molecule inhibitor, SAR405, caused alteration of cell polarity and disruption of epithelial
421 architecture by relieving LKB1 inhibition and triggering JNK activation (14). A role of Vps34 in
422 epithelial organization and polarity was also observed in 3D cultures of Caco-2 kidney cells
423 (14). It would be interesting to analyze the activation states of LKB1 and JNK in Vps34^{cKO}
424 thyroid, and, if modified, to cross Vps34^{cKO} with floxed LKB1 alleles.
425 The expression of the two SLC transporters, *Slc26a7* and *Slc26a4*, came out as a
426 surprise in Vps34^{cKO}. Decreased expression of Slc26a7 (4-fold) in Vps34^{cKO} may affect entry of
427 iodine in the thyroid. However, it should be mentioned that this alternative basolateral
428 transporter, SLC26A7, may only play an indirect role on iodine uptake (3). In addition,
429 expression of the main transporter, *Nis*, is at least 16-fold more important than that of
430 *Slc26a7*. This may explain why ^{125}I uptake was not affected. Expression of apical *Slc26a4*
431 (pendrin) in Vps34^{cKO} was even more dramatic with a 20-fold increase in expression. However,
432 we do not think that this would have affected apical transport of iodine. Indeed, in control
433 thyroids, expression level of *Slc26a4* were 60-fold less important than those of *anoctamin1* (6
434 Ct). This supports a more prominent role for *anoctamin1* in iodine apical transport, as
435 demonstrated by Twyffels (36). These changes in expression of *Slc26a7* and *Slc26a4* could

436 however impact on thyrocyte ion balance. Indeed, SLC26A7 and SLC26A4 transporters have
437 opposite action on chloride ions at the basolateral and apical membranes, respectively.
438 Decreased levels of SLC26A7 at the basolateral membrane may decrease the export of
439 chloride out of the thyrocyte (3). On the contrary the increase of SLC26A4 at the apical
440 membrane may increase the entry of chloride in the thyrocyte. Accumulation of chloride may
441 in turn decrease intracellular pH and causes cellular stress in Vps34^{cKO}.

442 The weak PAS staining in Vps34^{cKO} could be due to decreased exocytosis of Tg or
443 increased Tg endocytosis. We indeed very often observed intracellular Tg in Vps34^{cKO}. We
444 suggest that the defective process is the endocytic route rather than exocytosis because we
445 readily observed intracellular structures positive for iodinated Tg. This is rarely the case in
446 control thyrocyte where I-Tg is rapidly proteolytically processed. In addition, our work also
447 evidenced increased abundance and size of LAMP-1-positive late endosomes/lysosomes in
448 Vps34^{cKO} thyrocytes, with accumulation of Tg and the autophagic marker, p62, indicative of a
449 defective lysosomal trafficking and/or function. In addition to impaired Tg iodination, low T_4
450 plasma levels thus also probably result from impaired endocytic transport of iodo-Tg to
451 lysosomes and/or proteolytic excision of T_3/T_4 therein. Several studies have reported a role
452 for Vps34 in endocytic trafficking to lysosomes (13, 15, 30, 37) and activation of lysosomal
453 proteases (15). In our study on Vps34^{cKO} kidney PTCs, we also observed enlargement of
454 lysosomes and their filling by undigested material, labelled for a variety of antigens (19). In
455 Vps34^{cKO} thyrocytes, we also observed increased abundance and size of LAMP-1-positive
456 compartments filled with Tg and I-Tg. Based on these and previous findings showing that
457 Vps34 deletion leads to late endosome/lysosome enlargement and defective lysosomal
458 function (37), we assume a defective proteolytic excision of T_3/T_4 from iodo-Tg, analogous to
459 what we reported in cystinotic *Ctns*$^{-/-}$ mice (38). Cystinosis is a lysosomal storage disease due

460 to deletion or inactivating mutations of the lysosomal cystine transporter, cystinosin (39).
461 Defective cystinosin impacts on lysosomal proteolysis, presumably due to endolysosomal
462 mislocalization, impaired pro-cathepsin maturation and altered luminal redox status;
463 autophagic flux is also altered (40). Like cystinotic patients, *Ctns*$^{-/-}$ mice show compensated
464 hypothyroidism with moderate increase of TSH, thyrocyte hyperplasia and proliferation,
465 combined with progressive colloid depletion and evidence of increased endocytosis into
466 colloid droplets. Iodo-thyroglobulin could be detected in *Ctns*$^{-/-}$ but not wild-type thyrocyte
467 lysosomes, under identical labelling conditions, further indicating defective proteolysis.

468 It has recently become clear that Vps34 may act on lysosome positioning, which is
469 crucial to autophagosome formation (41,42). Similar to the kidney PTC defect, we observed
470 an increased p62 signal in Vps34^{cKO} thyroids at P14. Accumulation of p62 and LC3b in Vps34^{cKO}
471 indicates a block in the autophagy process. In addition, p62 accumulation also suggests
472 activation of the antioxidant NRF2 pathway by competitive binding of p62 to KEAP1 (33). We
473 indeed observed increased expression of two NRF2 target genes, namely the quinone
474 reductase, *Nqo1*, and the thioredoxin reductase 1, *Txnrd1*. Considering the expected key role
475 of Vps34 in macroautophagy, our data on mitophagy do not prove, but are compatible with
476 the suggestion that this important homeostatic process is abrogated upon Vps34 deficiency.

477 A final observation deserving discussion is the occurrence of viable cells in the follicular
478 lumens of Vps34^{cKO} thyroids. Our first hypothesis was that defective endocytic and autophagic
479 routes to the lysosomes could impact thyrocyte homeostasis, thus causing cellular stress.
480 Cellular stress, induced by defective autophagosome and lysosomal function, or by activation
481 of stress kinase such as JNK, could explain shedding of thyrocytes cells into the colloidal space.
482 However, luminal cells of Vps34^{cKO} thyroids were negative for E-cadherin and the thyrocyte-
483 specific transcription factor, TTF-1. Furthermore, lineage tracing experiments demonstrated

484 that these luminal cells had never expressed Pax8 and thus did not derive from thyrocytes.
485 The second hypothesis was that the cellular stress and loss of tissue homeostasis would recruit
486 macrophages. Indeed, we found that luminal cells were labelled for the conventional
487 macrophage marker, F4/80, are proliferating and display high LAMP-1 signal. In addition, Tg
488 and I-Tg colocalized with the LAMP-1 structures. This observation contributes to explain the
489 colloid exhaustion observed in Vps34^{cKO} and could thus be responsible for the low levels of
490 circulating T_4. Although the signal(s) attracting macrophages to the colloid is(are) unknown,
491 the loss of tight junction integrity might facilitate their invasion.

492 ***Acknowledgements***

493 This work was supported by grants from the Fonds pour la Recherche Scientifique (F.R.S-FNRS,
494 # J.0076.18, Belgium), Université catholique de Louvain (Actions de Recherche concertées to
495 CEP, ARC 15/20-065), and Fondation Roi Baudouin. SR and X-HL were supported by a grant
496 DK15070 from the National Institutes of Health, USA. Work in the laboratory of BV was
497 supported by grants from the MRC (G0700755) and BBSRC (BB/I007806/1; BB/M013278/1).
498 The core facility for Imaging Cells and Tissues was also financed by National Lottery, Région
499 bruxelloise, Région wallonne, Université catholique de Louvain and de Duve Institute. The
500 authors thank Prof. C. Ris-Stalpers for iodo-thyroglobulin antibody, Abdelkadder El Kaddouri
501 and Claude Massart for technical help. GG held a fellowship from the Fonds pour la formation
502 à la Recherche dans l'Industrie et l'Agriculture (FRIA, Belgium), TW was postdoctoral
503 researcher supported by UCLouvain, OD is supported by Télévie, VJ by the Cystinosis Research
504 Foundation, CS is a UCLouvain teaching assistant, HGC was a postdoctoral researcher and CEP
505 is a Senior Research Associate at F.R.S-FNRS.

506 ***Author disclosures and contributions***

507 BV is a consultant for Karus Therapeutics (Oxford, UK), iOnctura (Geneva, Switzerland) and
508 Venthera (Palo Alto, US) and has received speaker fees from Gilead. The other authors have
509 no competing financial interest. GG and TSW performed the initial morphological and
510 molecular studies and analyzed the data. OD and CS performed all the other experiments
511 and prepared the figures for the revision. VJ and AS participated in data collection and
512 analysis. HGC was involved in supervision of GG. BB and BV provided the Vps34 mice, XHL
513 and SR assayed T_4 and TSH levels, and CM provided expertise with ^{125}I experiments. PJC and
514 CEP conceived, designed and supervised the project, and wrote the manuscript. All authors
515 have approved the final version of the manuscript.

516 ***Name and address of corresponding author***

517 Prof. Christophe E. Pierreux
518 Cell Biology Unit
519 de Duve Institute and Université Catholique de Louvain
520 75, Avenue Hippocrate
521 B-1200 Brussels
522 Belgium
523 Email: christophe.pierreux@uclouvain.be

524 ***References***

525 1. Colin IM, Denef JF, Lengele B, Many MC, Gerard AC 2013 Recent insights into the cell biology
526 of thyroid angiofollicular units. Endocr Rev 34:209-238.

527 2. Carvalho DP, Dupuy C 2017 Thyroid hormone biosynthesis and release. Mol Cell Endocrinol
528 458:6-15.
529 3. Cangul H, Liao X-H, Schoenmakers E, Kero J, Barone S, Srichomkwun P, Iwayama H, Serra
530 EG, Saglam H, Eren E, Tarim O, Nicholas AK, Zvetkova I, Anderson CA, Karet Frankl FE,
531 Boelaert K, Ojaniemi M, Jääskeläinen J, Patyra K, Löf C, Williams ED, UK10K Consortium,
532 Soleimani M, Barrett T, Maher ER, Chatterjee VK, Refetoff S, Schoenmakers N 2018
533 Homozygous loss-of-function mutations in SLC26A7 cause goitrous congenital
534 hypothyroidism. J Clin Ivest Insight 3:e99631.
535 4. Koumarianou P, Gomez-Lopez G, Santisteban P 2017 Pax8 controls thyroid follicular polarity
536 through cadherin-16. J Cell Sci 130:219-231.
537 5. Shivas JM, Morrison HA, Bilder D, Skop AR 2010 Polarity and endocytosis: reciprocal
538 regulation. Trends Cell Biol 20:445-452.
539 6. Rodriguez-Boulan E, Macara IG 2014 Organization and execution of the epithelial polarity
540 programme. Nat Rev Mol Cell Biol 15:225-242.
541 7. Morrison HA, Dionne H, Rusten TE, Brech A, Fisher WW, Pfeiffer BD, Celniker SE, Stenmark
542 H, Bilder D 2008 Regulation of early endosomal entry by the Drosophila tumor
543 suppressors Rabenosyn and Vps45. Mol Biol Cell 19:4167-4176.
544 8. Bilanges B, Posor Y, Vanhaesebroeck B 2019 PI3K isoforms in cell signaling and vesicle
545 trafficking. Nat Rev Mol Cell Biol May 20. doi: 10.1038/s41580-019-0129-z. [Epub
546 ahead of print].
547 9. Lindmo K, Stenmark H 2006 Regulation of membrane traffic by phosphoinositide 3-kinases.
548 J Cell Sci 119:605-614.

549 10. Juhasz G, Hill JH, Yan Y,Sass M, Baehrecke EH, Backer JM, Neufeld TP 2008 The class III
550 PI(3)K Vps34 promotes autophagy and endocytosis but not TOR signaling in Drosophila.
551 J Cell Biol 181:655-666.
552 11. Backer JM 2008 The regulation and function of Class III PI3Ks: novel roles for Vps34.
553 Biochem J 410:1-17.
554 12. Jaber N, Zong WX 2013 Class III PI3K Vps34: essential roles in autophagy, endocytosis, and
555 heart and liver function. Ann NY Acad Sci 1280:48-51.
556 13. Bechtel W, Helmstädter M, Balica J, Hartleben B, Kiefer B, Hrnjic F, Schell C, Kretz O, Liu S,
557 Geist F, Kerjaschki D, Walz G, Huber TB 2013 Vps34 deficiency reveals the importance
558 of endocytosis for podocyte homeostasis. J Am Soc Nephrol 24:727-743.
559 14. O'Farrell F, Lobert VH, Sneeggen M, Jain A, Katheder NS, Wenzel EM, Schultz SW, Tan KW,
560 Brech A, Stenmark H, Rusten TE 2017 Class III phosphatidylinositol-3-OH kinase
561 controls epithelial integrity through endosomal LKB1 regulation. Nat Cell Biol 19:1412-
562 1423.
563 15. Ronan B, Flamand O, Vescovi L, Dureuil C, Durand L, Fassy F, Bachelot M-F, Lamberton A,
564 Mathieu M, Bertrand T, Marquette J-P, El-Ahmad Y, Filoche-Romme B, Schio L, Garcia-
565 Echeverria C, Goulaouic H, Pasquier B 2014 A highly potent and selective Vps34
566 inhibitor alters vesicle trafficking and autophagy. Nat Chem Biol 10:1013-1019.
567 16. Nascimbeni AC, Codogno P, Morel E 2017 Phosphatidylinositol-3-phosphate in the
568 regulation of autophagy membrane dynamics. FEBS J 284:1267-1278.
569 17. Dupont N, Nascimbeni AC, Morel E, Codogno P 2017 Molecular Mechanisms of
570 Noncanonical Autophagy. Intl Rev Cell Mol Biol 328:1-23.
571 18. Carpentier S, N'Kuli F, Grieco G, Van Der Smissen P, Janssens V, Emonard H, Bilanges B,
572 Vanhaesebroeck B, Gaide Chevronnay HP, Pierreux CE, Tyteca D, Courtoy PJ 2013

573 ClassIII phosphoinositide 3-kinase/VPS34 and dynamin are critical for apical endocytic
574 recycling. Traffic 14:933-948.
575 19. Grieco G, Janssens V, Gaide Chevronnay HP, N'Kuli F, Van Der Smissen P, Wang TS, Shan J,
576 Vainio S, Bilanges B, Jouret F, Vanhaesebroeck B, Pierreux CE, Courtoy PJ 2018
577 Suppression of Vps34 PI 3-kinase activity in kidney proximal tubules abrogates apical
578 trafficking and causes a Fanconi syndrome. Sci Rep 8:14133.
579 20. Shan J, Jokela T, Skovorodkin I, Vainio S 2010 Mapping of the fate of cell lineages generated
580 from cells that express the Wnt4 gene by time-lapse during kidney development.
581 Differentiation 79:57-64.
582 21. Bouchard M, Souabni A, Busslinger M 2004 Tissue-specific expression of cre recombinase
583 from the Pax8 locus. Genesis 38:105-109.
584 22. Valet C, Levade M, Chicanne G, Bilanges B, Cabou C, Viaud J, Gratacap MP, Gaits-Iacovoni
585 F, Vanhaesebroeck B, Payrastre B, Severin S 2017 A dual role for the class III PI3K,
586 Vps34, in platelet production and thrombus growth. Blood 130:2032-2042.
587 23. Pohlenz J, Maqueem A, Cua K, Weiss RE, Van Sande J, Refetoff S 1999 Improved
588 radioimmunoassay for measurement of mouse thyrotropin in serum: strain
589 differences in thyrotropin concentration and thyrotroph sensitivity to thyroid
590 hormone. Thyroid 9:1265-1271.
591 24. Delmarcelle AS, Villacorte M, Hick AC, Pierreux CE 2014 An ex vivo culture system to study
592 thyroid development. J Vis Exp 6:88.
593 25. Hick AC, Delmarcelle AS, Bouquet M, Klotz S, Copetti T, Forez C, Van Der Smissen P,
594 Sonveaux P, Collet JF, Feron O, Courtoy PJ, Pierreux CE 2013 Reciprocal
595 epithelial:endothelial paracrine interactions during thyroid development govern
596 follicular organization and C-cells differentiation. Dev Biol 381:227-240.

597 26. Dupasquier S, Delmarcelle AS, Marbaix E, Cosyns JP, Courtoy PJ, Pierreux CE 2014
598 Validation of housekeeping gene and impact on normalized gene expression in clear
599 cell renal cell carcinoma: critical reassessment of YBX3/ZONAB/CSDA expression. BMC
600 Mol Biol 15:9.
601 27. Massart C, Hoste C, Virion A, Ruf J, Dumont JE, Van Sande J 2011 Cell biology of H2O2
602 generation in the thyroid: investigation of the control of dual oxidases (DUOX) activity
603 in intact ex vivo thyroid tissue and cell lines. Mol Cell Endocrinol 343:32-44.
604 28. Zhou X, Takatoh J, Wang F 2011 The mammalian class 3 PI3K (PIK3C3) is required for early
605 embryogenesis and cell proliferation. PloS one 6:e16358.
606 29. Chen J, Chen MX, Fogo AB, Harris RC, Chen JK 2013 mVps34 deletion in podocytes causes
607 glomerulosclerosis by disrupting intracellular vesicle trafficking. J Am Soc Nephrol.
608 24:198-207.
609 30. Bechtel, W, Helmstädter M, Balica J, Hartleben B, Schell C, Huber TB 2013 The class III
610 phosphatidylinositol 3-kinase PIK3C3/VPS34 regulates endocytosis and
611 autophagosome-autolysosome formation in podocytes. Autophagy 9:1097-1099.
612 31. Cohen-Kaplan V, Ciechanover A, Livneh I 2016 p62 at the crossroad of the ubiquitin-
613 proteasome system and autophagy. Oncotarget 7:83833-83834.
614 32. Bjorkoy G, Lamark T, Pankiv S, Overvatn A, Brech A, Johansen T 2009 Monitoring
615 autophagic degradation of p62/SQSTM1. Methods Enzymol 452:181-197.
616 33. Ziros PG, Habeso IG, Chartoumpekis DV, Ntalampyra E, Somm E, Renaud CO, Bongiovanni
617 M, Trougakos IP, Yamamoto M, Kensler TW, Santisteban P, Carrascao N, Ris-Stalpers
618 C, Amendola E, Liao XH, Rossich L, Thomasz L, Juvenal GJ, Refetoff S, Sykiotos GP 2018
619 NFE2-related transcription factor 2 coordinates antioxidant defense with thyroglobulin
620 production and iodination in the thyroid gland. Thyroid 28:780-798.

621 34. Grasberger H, De Deken X, Mayo OB, Raad H, Weiss M, Liao XH, Refetoff S 2012 Mice
622 deficient in dual oxidase maturation factors are severely hypothyroid. Mol Endocrinol
623 26:481-492.
624 35. Christophe-Hobertus C, Christophe D 2010 Delimitation and functional characterization of
625 the bidirectional THOX-DUOXA promoter regions in thyrocytes. Mol Cell Endocrinol
626 317:161-167.
627 36. Twyffels L, Strickaert A, Virreira M, Massart C, Van Sande J, Wauquier C, Beauwens R,
628 Dumont JE, Galietta LJ, Boom A, Kruys V 2014 Anoctamin-1/TMEME16A is the major
629 apical iodide channel of the thyrocyte. Am J Physiol Cell Physiol 307:1102-1112.
630 37. Jaber N, Mohd-Naim N, Wang Z, DeLeon JL, Kim S, Zhong H, Sheshadri N, Dou Z, Edinger
631 AL, Du G, Braga VM, Zong WX 2016 Vps34 regulates Rab7 and late endocytic trafficking
632 through recruitment of the GTPase-activating protein Armus. J Cell Sci 129:4424-4435.
633 38. Gaide Chevronnay HP, Janssens V, Van Der Smissen P, Liao XH, Abid Y, Nevo N, Antignac
634 C, Refetoff S, Cherqui S, Pierreux CE, Courtoy PJ 2015 A mouse model suggests two
635 mechanisms for thyroid alterations in infantile cystinosis: decreased thyroglobulin
636 synthesis due to endoplasmic reticulum stress/unfolded protein response and
637 impaired lysosomal processing. Endocrinology 156:2349-2364.
638 39. Gahl WA, Thoene JG, Schneider JA 2002 Cystinosis. N Engl J Med. 347:111–121.
639 40. Cherqui S, Courtoy PJ 2017 The renal Fanconi syndrome in cystinosis: pathogenic insights
640 and therapeutic perspectives. Nat Rev Nephr 13:115-131.
641 41. Hong Z, Pedersen NM, Wang L, Torgersen ML, Stenmark H, Raiborg C 2017 PtdIns3P
642 controls mTORC1 signaling through lysosomal positioning. J Cell Biol 216:4217-4233.
643 42. Korolchuk VI, Rubinsztein DC 2011 Regulation of autophagy by lysosomal positioning.
644 Autophagy 7:927-928.

645 **Figure legends**

646

647 ***Figure 1. Genetic and histopathological characterization. A. Extensive genetic excision of***
648 ***Vps34 exon 21***. Compared with control (black boxes), Vps34^{cKO} thyroid (red boxes) shows ~70%
649 reduction in exon 21 mRNA level at P14. The unchanged mRNA level spanning exons 22-24
650 serves as control. Boxes with median and percentiles of 10 WT and 11 cKO samples; ***, p<
651 0.0001 by Mann-Whitney non-parametric test. ***B. Increased thyroid weight.*** Compared with
652 control (black boxes), Vps34^{cKO} thyroid (red boxes) shows a two-fold increase in thyroid weight.
653 Boxes with median and percentiles of 8 WT and 6 cKO samples; **, p< 0.01 by Mann-Whitney
654 non-parametric test. ***C. Histopathological evidence for colloid exhaustion.*** As compared to
655 control thyroid tissues (n=3) where all follicles show regular lumen filling with homogenous
656 and intense PAS (Periodic Acid Shiff) staining, Vps34^{cKO} thyroids (n=3) present fewer, mostly
657 centrally located, PAS-stained follicles and with weaker staining intensity, other follicles that
658 appear empty (for further quantification, see Supplementary Figure 1). ***D. Vps34^{cKO} thyrocytes***
659 ***are altered and follicles contains abundant non-epithelial cells***. Nuclei are labeled by Hoechst
660 (shown in white); thyrocyte basolateral contours are labeled for E-cadherin (red); two lumen
661 boundaries are delineated by broken lines. As compared to control thyroid follicles, Vps34^{cKO}
662 follicular structures are frequently irregular and containing additional cells inside the lumen
663 (arrowheads). These cells are not labeled for E-cadherin.

664

665 ***Figure 2. Vps34^{cKO} mice display severe hypothyroidism associated with high TSH levels.*** As
666 compared to control mice (black boxes), T_4 plasma level in Vps34^{cKO} is extremely low (red
667 boxes). Conversely, TSH levels are dramatically elevated. (10 WT and 9 cKO samples; ***, p=
668 0.0003 by Mann-Whitney non-parametric test).

669 ***Figure 3. Relative expression level of main actors of thyroid hormonogenesis at P14***. Gene
670 expression analysis by RT-qPCR, presented as boxes with median and percentiles. As
671 compared to control thyroid (black boxes), expression in Vps34^{cKO} (red boxes) is preserved for
672 the thyroid-specific genes *Nis*, *Tpo*, *Tg* and *Duox2.* Expression of the TSH receptor (*Tshr*) and
673 of *Slc26a4* is significantly increased in Vps34^{cKO}, while expression of *Slc26a7* and *Duoxa2* is
674 significantly decreased. Boxes with median and percentiles of at least 9 control and 9 Vps34^{cKO}
675 samples; ***, p< 0.001 by Mann-Whitney non-parametric test.
676
677 ***Figure 4. Normal uptake of iodine but major defect of organification in Vps34^{cKO} thyroid. A.***
678 Comparable ^{125}I-iodine uptake in the thyroid in control genotypes (black box) and Vps34^{cKO}
679 thyroid (red box), but much reduced ^{125}I bound to protein (in %) in Vps34^{cKO} thyroid,
680 suggesting defective organification. Boxes with median and percentiles of 39 (10 Flox/+, 19
681 Flox/Flox, 10 Cre;Flox/+) and 12 Vps34^{cKO} (Cre;Flox/Flox) samples; ***, p< 0.001 by Mann-
682 Whitney non-parametric test. **B**. Level of H_2O_2 in total thyroid extracts show a trend to an
683 increase in Vps34^{cKO} thyroid. Boxes with median and percentiles of 9 control and 9 Vps34^{cKO}
684 samples; p= 0.077 by Mann-Whitney non-parametric test.
685
686 ***Figure 5. Normal basolateral but impaired apical organization of tyrocytes. A.*** Thyroid
687 sections from control (left) and Vps34^{cKO} (right) labeled for laminin (red), ezrin (green) and E-
688 cadherin (white). Nuclei are labeled by Hoechst (shown in blue). In control thyroid, laminin
689 surrounds follicles composed of thyrocytes delineated by basolateral E-cadherin and apical
690 ezrin. In Vps34^{cKO}, laminin normally surrounds follicles composed of thyrocytes with well-
691 defined basolateral E-cadherin but weaker and less regular apical ezrin. Note here apical
692 membrane bulging in the colloidal space. ***B.*** Thyroid sections from control (left) and Vps34^{cKO}

693 (right) labeled for ZO-1 (red), Na^+/K^+-ATPase (green) or β-catenin (white). Nuclei are labeled
694 by Hoechst (shown in blue). In control and $Vps34^{cKO}$ thyroid, Na^+/K^+-ATPase and β-catenin are
695 correctly localized and restricted to the basolateral pole of the thyrocytes, indicating the
696 presence of a tight junction. However, the tight junction-associated protein ZO-1 is only
697 detected at few apico/basolateral junctions.
698
699 ***Figure 6. Evidence for defective iodide organification in $Vps34^{cKO}$ thyroid: follicular lumina***
700 ***with Tg but devoid of iodinated-Tg.*** **A.** Thyroid sections from control (left) and $Vps34^{cKO}$ (right)
701 labeled for E-cadherin (green) and thyroglobulin (red), recognized either for a core protein
702 epitope (Tg), or a hormonogenic peptide (I-Tg). Control follicular lumina are round and
703 uniformly labeled for both Tg and I-Tg. In $Vps34^{cKO}$, follicular structures are less regular, with
704 the majority containing Tg, but not the hormonogenic peptide. In $Vps34^{cKO}$, two serial (tilted)
705 sections are shown. ***B. Comparison of Tg labelling in control and $Vps34^{cKO}$ thyrocytes.*** In control
706 follicles, Tg is essentially restricted to lumen, with little or no signal inside thyrocytes. In
707 $Vps34^{cKO}$, Tg is readily detected within thyrocytes as collections of submicrometric dots or
708 larger spheres (arrowheads). Of note, some luminal cells (broken line in middle panel) also
709 contain Tg-labeled spheres, indicating active endocytosis (arrow).
710
711 ***Figure 7. $Vps34^{cKO}$ thyrocytes display increased LAMP-1 signal and impaired I-Tg proteolytic***
712 ***processing.*** **A.** Thyroid sections from control (left) and $Vps34^{cKO}$ (right) labeled for
713 thyroglobulin (red), E-cadherin (green) and lysosomal LAMP-1 (white). Nuclei are labeled by
714 Hoechst (shown in blue). In control, thyrocytes rarely contain intracellular Tg and LAMP-1
715 signal is weak. In $Vps34^{cKO}$, most thyrocytes have intracellular Tg (arrowheads) and LAMP-1
716 signal is much increased. Insets show magnification with separate emissions, then merged,

717 channels. Note colocalization of Tg with LAMP-1 in luminal cells (at right). **B.** Thyroid sections
718 from control (left) and Vps34^{cKO} (right) labeled for iodinated-thyroglobulin (I-Tg, red), E-
719 cadherin (green) and lysosomal LAMP-1 (white). Nuclei are labeled by Hoechst (shown in blue).
720 As compared to control follicles which show a weak signal for LAMP-1, and rare intracellular I-
721 Tg, LAMP-1 signal is intense in Vps34^{cKO} thyrocytes and intracellular I-Tg dots are frequently
722 observed (arrowheads). As shown in the enlargements below, LAMP-1-labeled structures in
723 Vps34^{cKO} thyrocytes are enlarged or vacuolated as compared to control.
724
725 ***Figure 8. Vps34^{cKO} thyrocytes show strong accumulation of p62 and LC3b dots.*** **A.** Thyroid
726 sections from control (left) and Vps34^{cKO} (right) labeled for p62 (red), LC3b (green) and
727 lysosomal LAMP-1 (white). Nuclei are labeled by Hoechst (shown in blue). Compared with
728 control follicles, which show low LAMP-1 and almost no signal for p62 and LC3b, all three
729 markers are very strong in Vps34^{cKO} thyroid sections. p62 perfectly co-localizes with LC3b and
730 labels large aggregates. These aggregates are adjacent to LAMP-1-positive structures. **B.**
731 **Increased NRF2 signaling.** Gene expression analysis by RT-qPCR, presented as boxes with
732 median and percentiles. As compared to control thyroid (black boxes), expression of *Nrf2* is
733 reduced in Vps34^{cKO} (red boxes), but level of two out of three NRF2 target genes, *Txnrd1* and
734 *Nqo1* is increased. Boxes with median and percentiles of at least 9 control and 9 Vps34^{cKO}
735 samples; *, $p< 0.05$ and ***, $p< 0,001$ by Mann-Whitney non-parametric test.
736
737 ***Figure 9. Luminal cells in Vps34^{cKO} thyroid are not thyrocytes. A.*** Immunolabelling for
738 thyrocyte transcription factor-1 (TTF-1, green); nuclei are visualized with the Hoechst stain
739 (shown in white). In both control and Vps34^{cKO} thyroid, nuclei of thyrocytes circumscribing the
740 follicular lumina are all labeled by the thyrocyte-specific transcription-factor-1, TTF-1. As

741 indicated by the arrowheads, nuclei of luminal cells show no signal for TTF-1 (only white signal
742 representing Hoechst). ***B.*** Immunolabelling for E-cadherin (red) and YFP (green); nuclei are
743 visualized with the Hoechst stain (shown in blue). Representative images of Vps34cKO thyroid
744 sections reveal expression of YFP only in cells surrounding the follicular lumina, i.e. in cells
745 where Pax8-Cre has been active. Luminal cells do not derive from thyrocyte progenitors as
746 they are negative for YFP.
747
748 ***Figure 10. Luminal cells in Vps34^{cKO} thyroid are macrophages. A.*** Immunolabelling for E-
749 cadherin (red), and for the conventional macrophage marker (F4/80, green); nuclei are
750 visualized with the Hoechst stain (shown in white). In Vps34^{cKO} thyroid, F4/80 signal can be
751 found in the interstitium (arrows), but also in the colloidal space, thus identifying luminal cells
752 as infiltrating macrophages. **D. Luminal cells are taking up the colloid.** Immunolabelling for I-
753 Tg (red), F4/80 (green) and LAMP-1 (white). Nuclei are visualized with the Hoechst stain
754 (shown in blue). Luminal cells in Vps34^{cKO} have abundant LAMP-1 structures that surround I-Tg
755 droplets. Arrowheads show additional I-Tg in thyrocytes. Broken lines indicate luminal
756 contours.
757

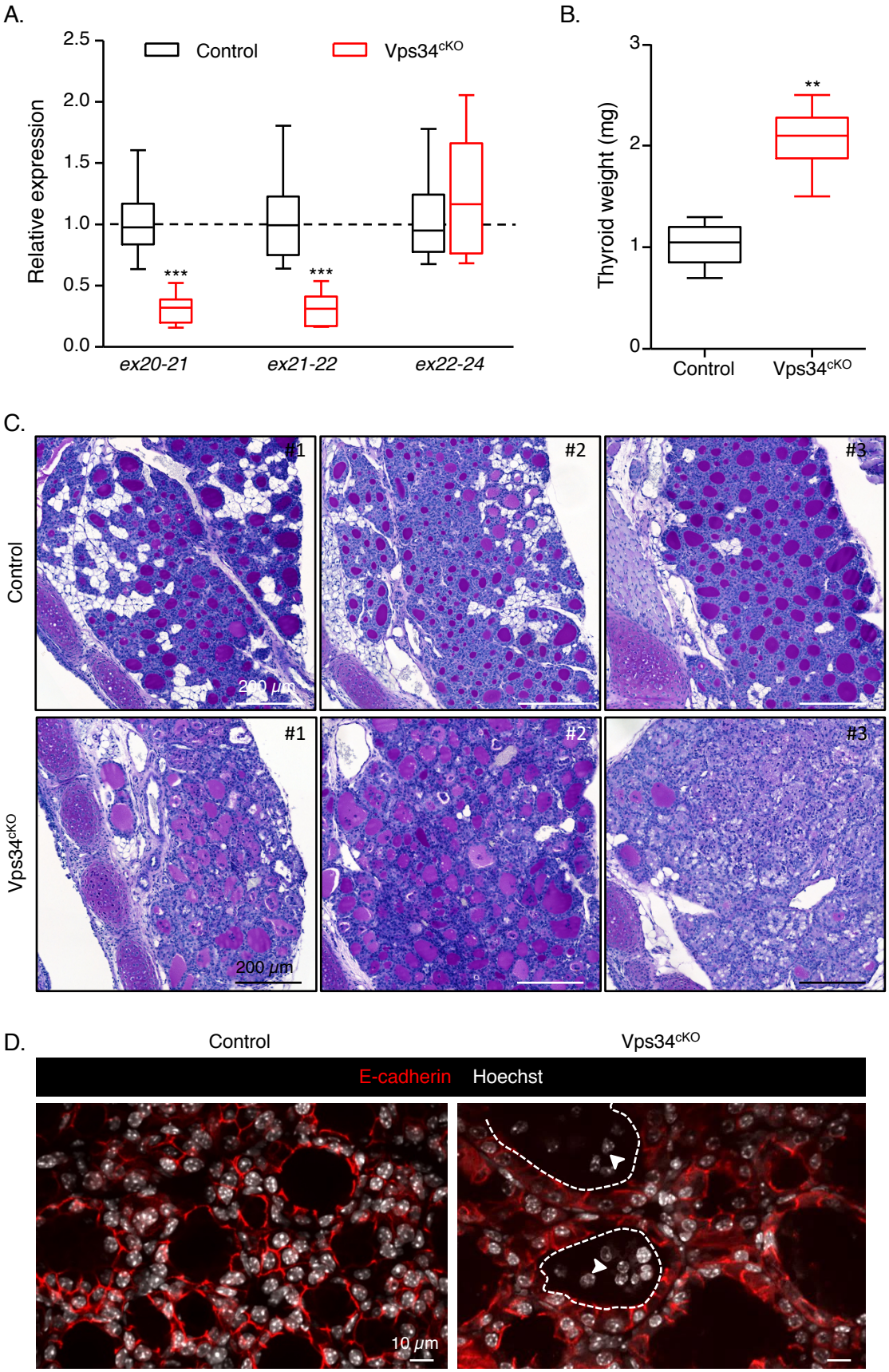
A.
Control
Vps34cKO
Relative expression
2.5
2.0
1.5
1.0
0.5
0.0
***
***
ex20-21
ex21-22
ex22-24
B.
Thyroid weight (mg)
3
2
1
0
**
Control
Vps34cKO
C.
Control
Vps34cKO
#1
#2
#3
200 µm
D.
Control
Vps34cKO
E-cadherin
Hoechst
10 µm

GriecoFig1

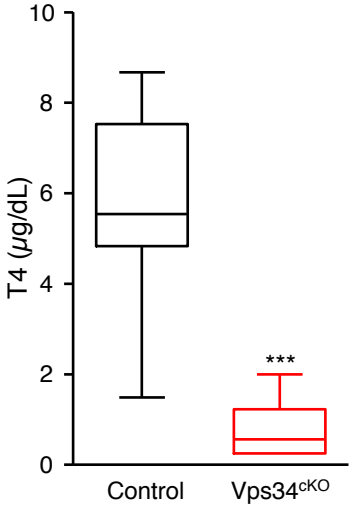
10
8
6
4
2
0
T4 (μg/dL)
***
Control
Vps34cKO

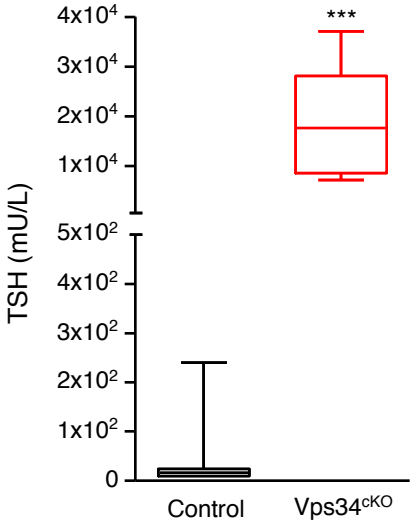
4x10^4
3x10^4
2x10^4
1x10^4
5x10^2
4x10^2
3x10^2
2x10^2
1x10^2
0
TSH (mU/L)
***
Control
Vps34cKO

GriecoFig2

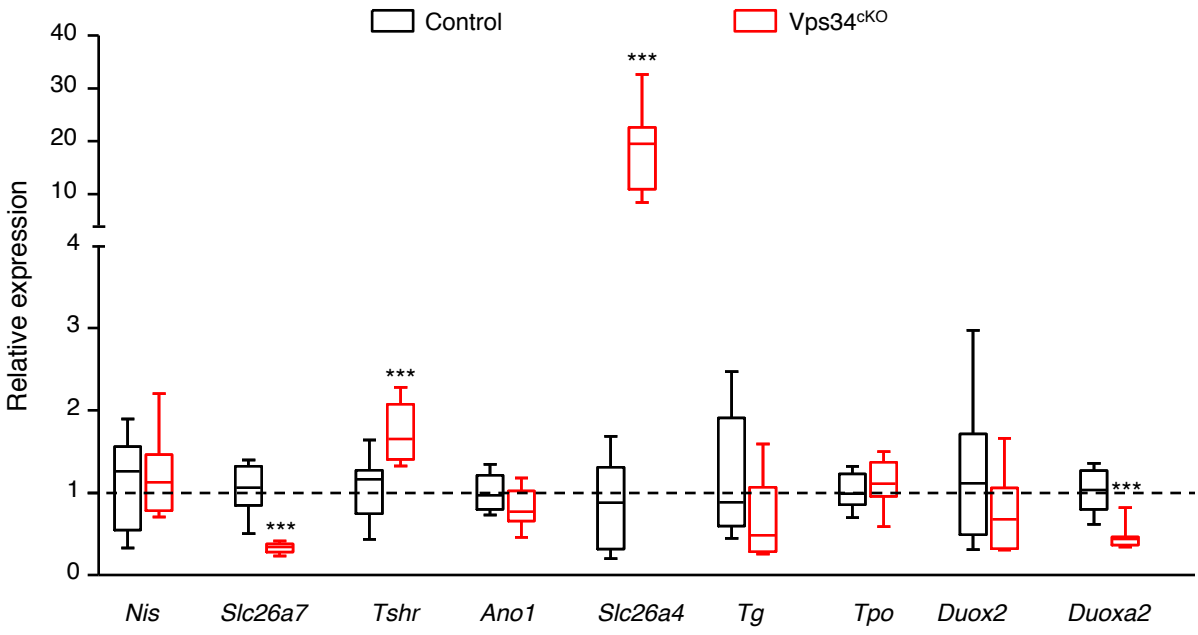
Control
Vps34cKO
Relative expression
40
30
20
10
4
3
2
1
0
***
***
***
***
Nis
Slc26a7
Tshr
Ano1
Slc26a4
Tg
Tpo
Duox2
Duoxa2

GriecoFig3

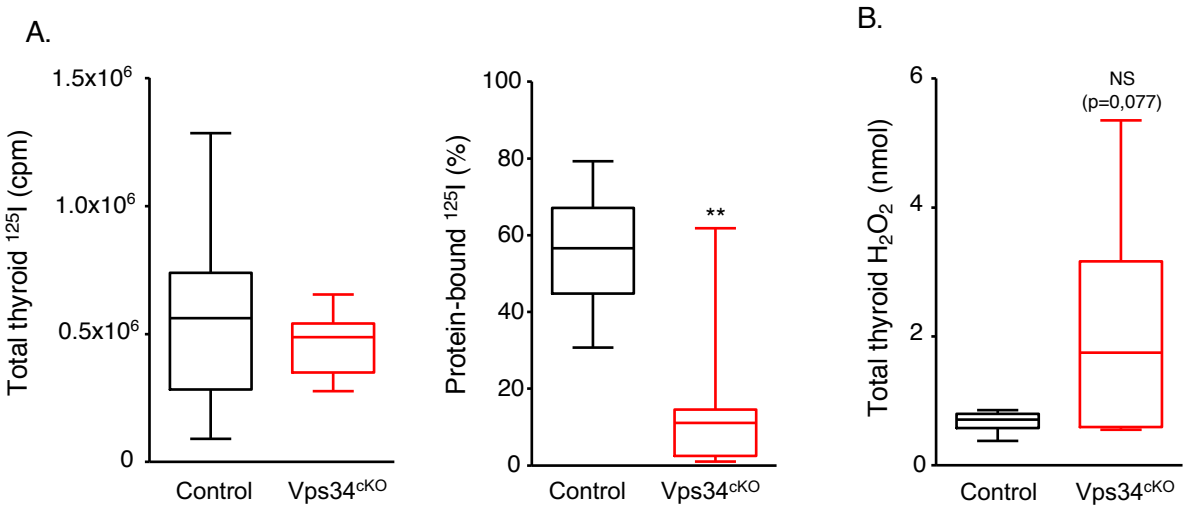
A.
Total thyroid 125I (cpm)
1.5x10^6
1.0x10^6
0.5x10^6
0
Control
Vps34cKO
Protein-bound 125I (%)
100
80
60
40
20
0
**
Control
Vps34cKO
B.
Total thyroid H2O2 (nmol)
6
4
2
0
NS
(p=0,077)
Control
Vps34cKO

GriecoFig4

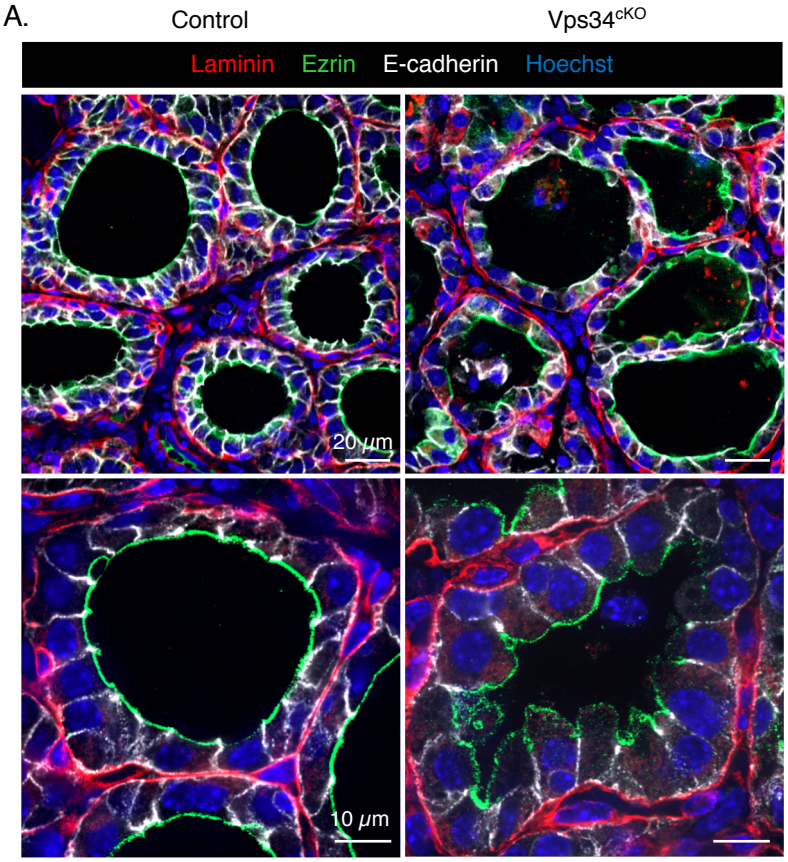
A.
Control
Vps34cKO
Laminin
Ezrin
E-cadherin
Hoechst
20 μm
10 μm

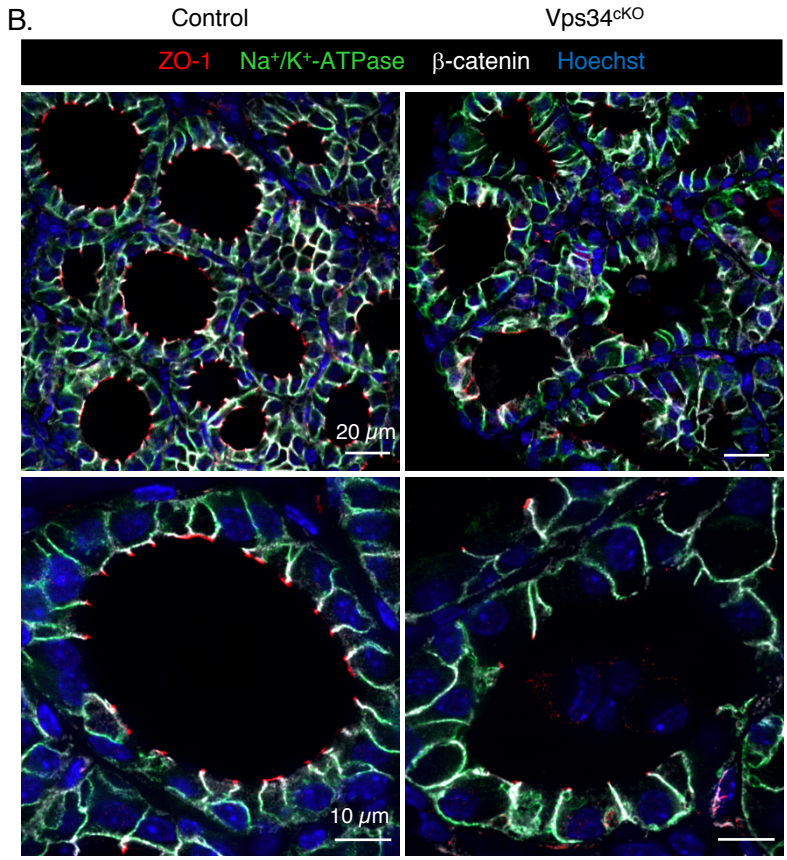
B.
Control
Vps34cKO
ZO-1
Na+/K+-ATPase
β-catenin
Hoechst
20 μm
10 μm

GriecoFig5

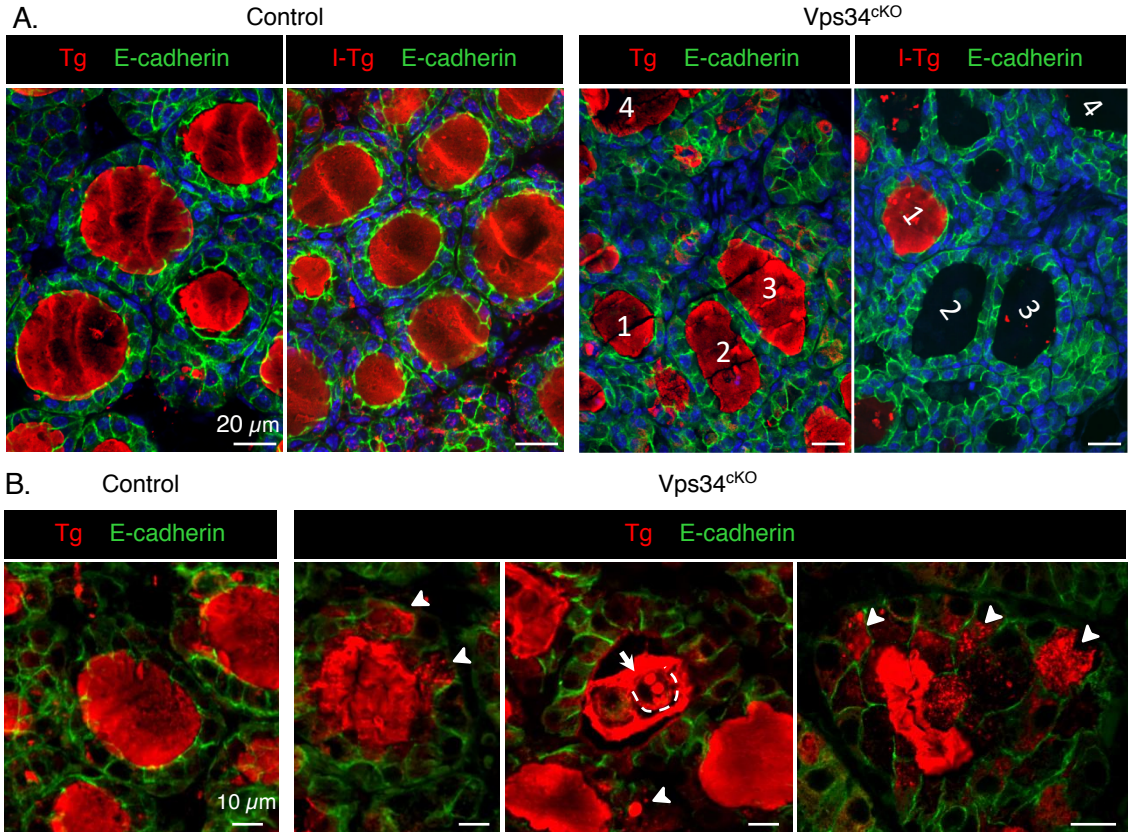
A.
Control
Vps34cKO
Tg E-cadherin
I-Tg E-cadherin
Tg E-cadherin
I-Tg E-cadherin
20 μm
1
2
3
4
B.
Control
Vps34cKO
Tg E-cadherin
Tg E-cadherin
10 μm

GriecoFig6

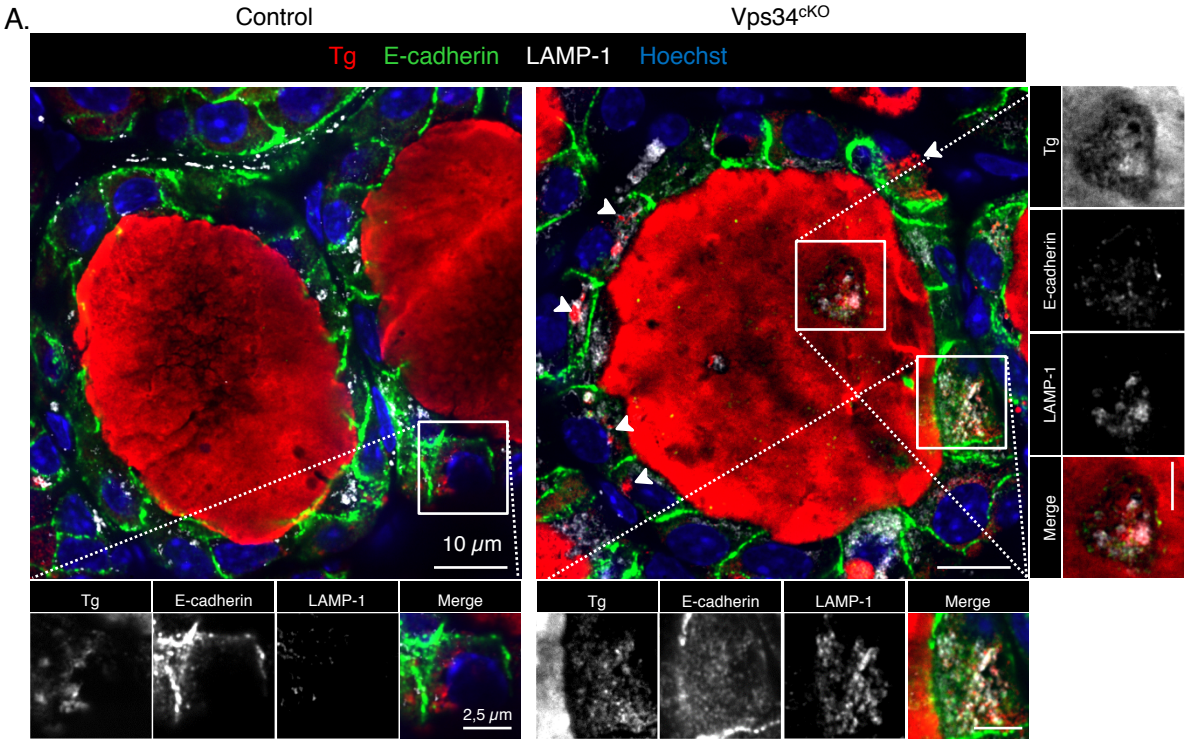
A.
Control
Vps34cKO
Tg E-cadherin LAMP-1 Hoechst
10 μm
Tg
E-cadherin
LAMP-1
Merge
2,5 μm

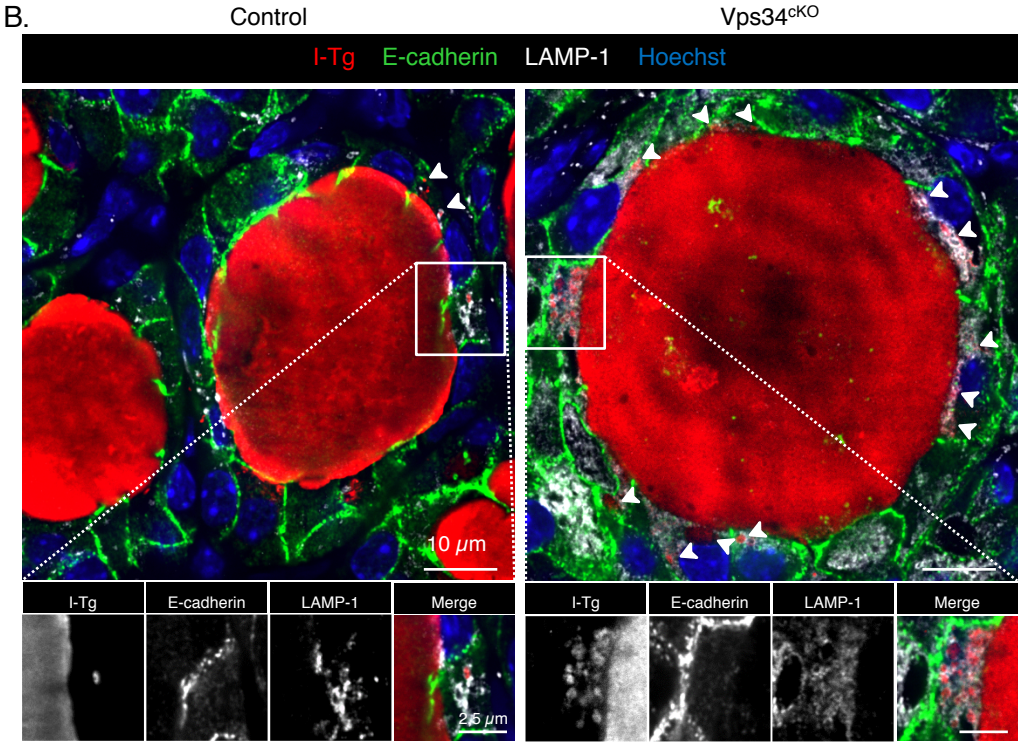
B.
Control
Vps34cKO
I-Tg E-cadherin LAMP-1 Hoechst
10 μm
I-Tg
E-cadherin
LAMP-1
Merge
2,5 μm

GriecoFig7

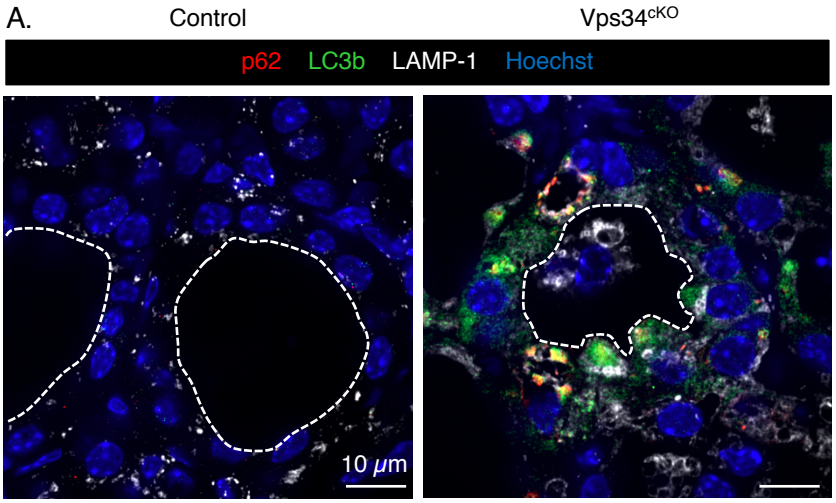
A.
Control
Vps34cKO
p62
LC3b
LAMP-1
Hoechst
10 μm

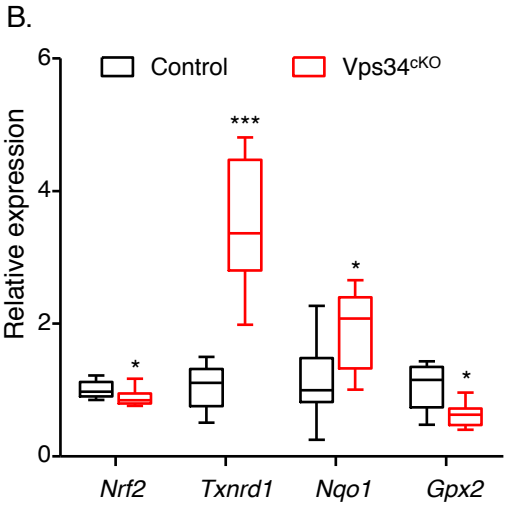
B.
Control
Vps34cKO
Relative expression
6
4
2
0
***
*
*
*
Nrf2
Txnrd1
Nqo1
Gpx2

GriecoFig8

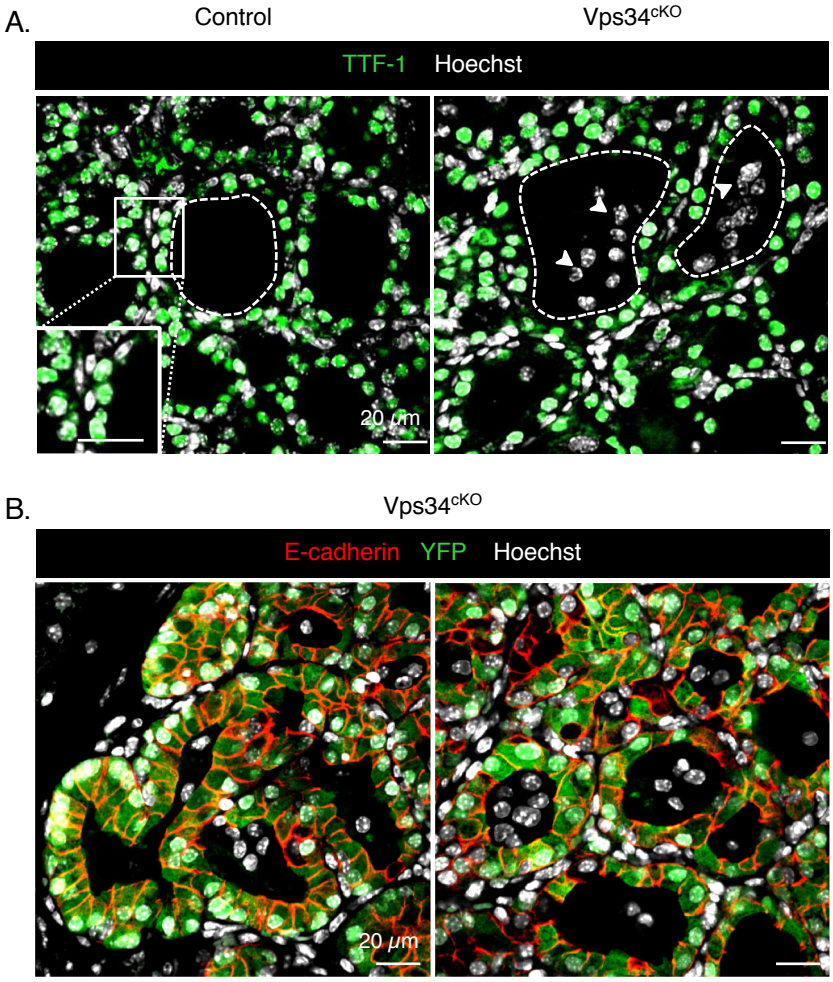
A.
Control
Vps34cKO
TTF-1 Hoechst
20 μm
B.
Vps34cKO
E-cadherin YFP Hoechst
20 μm

GriecoFig9

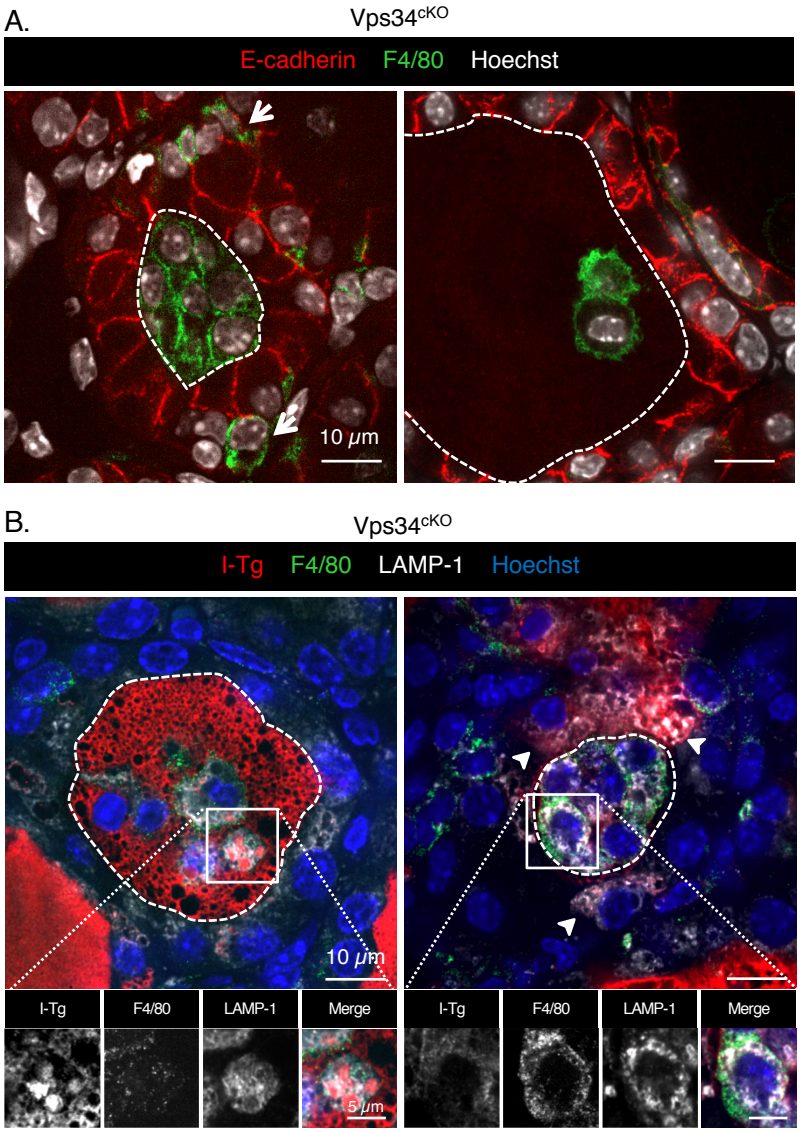

GriecoFig10